JTTEE5 15:598-603
DOI: 10.1361/105996306X146965
1059-9630/$19.00 © ASM International

Peer Reviewed

Characterization of YSZ Solid Oxide Fuel Cells Electrolyte Deposited by Atmospheric Plasma Spraying and Low Pressure Plasma Spraying

C. Zhang, H.-L. Liao, W.-Y. Li, G. Zhang, C. Coddet, C.-J. Li, C.-X. Li, and X.-J. Ning

(Submitted March 2, 2006; in revised form April 14, 2006)

Yttria doped zirconia has been widely used as electrolyte materials for solid oxide fuel cells (SOFC). Plasma spraying is a cost-effective process to deposit YSZ electrolyte. In this study, the 8 mol% Y_2O_3 stabilized ZrO_2 (YSZ) layer was deposited by low pressure plasma spraying (LPPS) and atmospheric plasma spraying (APS) with fused-crushed and agglomerated powders to examine the effect of spray method and particle size on the electrical conductivity and gas permeability of YSZ coating. The microstructure of YSZ coating was characterized by scanning electron microscopy and x-ray diffraction analysis. The results showed that the gas permeability was significantly influenced by powder structure. The gas permeability of YSZ coating deposited by fused-crushed powder is one order lower in magnitude than that by agglomerated powder. Moreover, the gas permeability of YSZ deposited by LPPS is lower than that of APS YSZ. The electrical conductivity of the deposits through thickness direction was measured by potentiostat/galvanostat based on three-electrode assembly approach. The electrical conductivity of YSZ coating deposited by low pressure plasma spraying with fused-crushed powder of small particle size was 0.043 S cm^{-1} at 1000 °C, which is about 20% higher than that of atmospheric plasma spraying YSZ with the same powder.

Keywords electrical conductivity, gas permeability, plasma spraying coating, solid oxide fuel cells (SOFC), YSZ electrolyte

1. Introduction

Solid oxide fuel cells (SOFC) have emerged as an alternative to conventional power generator due to their potential to reduce the environmental impact and high power generation efficiency. Solid oxide electrolyte layer is one of the basic components in SOFCs operating at a high temperature. To date, the doped zirconia, especially 8 mol% yttria doped zirconia (YSZ), is the most commonly used electrolyte material for its thermal stability, high ionic conductivity, and good thermal expansion compatibility with the other two electrodes materials (Ref 1, 2). Many different processes have been applied to fabricate YSZ electrolyte in the form of coating, including chemical vapor deposition (CVD), electrochemical vapor deposition (EVD), sol-gel, spray pyrolysis, thermal spraying, physical vapor deposition (PVD), tape-casting, and screen-printing techniques, and so on (Ref 3). Among those techniques, plasma-spraying process is a promising method to deposit electrolyte layer for its high deposition rate, cost effectiveness, and flexibility for automated production. Low pressure plasma spraying (LPPS) and atmospheric plasma spraying (APS) were two variations of plasma spraying used to deposit YSZ coating (Ref 4-6). It has been pointed out that LPPS YSZ is more feasible for SOFC than APS YSZ (Ref 7). A recent study also suggests that a SOFC of excellent performance can be achieved with LPPS YSZ (Ref 8). However, the higher cost of LPPS than APS makes APS more competitive than LPPS. A previous study suggests that the electrical conductivity of LPPS YSZ coating is compatible to APS YSZ. As a result, high performance of SOFC, composed of APS YSZ, is reported (Ref 9).

In this study, YSZ coatings were prepared by two plasma spraying processes using two different powders to examine controlling factors over YSZ properties in terms of gas permeability and electrical conductivity.

2. Experimental

2.1 Plasma Spraying of YSZ Samples

Two commercially available YSZ powders were used as feedstock materials. Table 1 shows the nominal compositions and size ranges of both powders, which are referred to as YSZ1 and YSZ2 in this study. YSZ1 was a fused-crushed powder (Plasmatex, Sulzer-Metco, Winterthor, Switzerland) and YSZ2 was an agglomerated powder containing nanoscale substructure of 25 nm (TZ8Y, TOSOH, Tokyo, Japan). Figure 1 illustrates the morphology of both powders. Compared with YSZ1 powder, YSZ2 powder has wider size distribution.

YSZ coatings were deposited with a VPS system (PT-3000

This article was originally published in *Building on 100 Years of Success, Proceedings of the 2006 International Thermal Spray Conference* (Seattle, WA), May 15-18, 2006, B.R. Marple, M.M. Hyland, Y.-Ch. Lau, R.S. Lima, and J. Voyer, Ed., ASM International, Materials Park, OH, 2006.

C. Zhang, H.-L. Liao, W.-Y. Li, G. Zhang, and **C. Coddet,** Laboratoire d'Etudes et de Recherches sur les Matériaux, les Procédés et les Surfaces, Université de Technologie de Belfort-Montbéliard, 90010, Belfort, France; **C. Zhang, C.-J. Li, C.-X. Li,** and **X.-J. Ning,** State Key Laboratory for Mechanical Behavior of Materials, Xi'an Jiaotong University, 710049, Shaanxi, China. Contact e-mail: hanlin.liao@utbm.fr.

Table 1 Powders used for plasma spraying

Powder code	YSZ1	YSZ2
Manufacturing process	Fused-crushed	Agglomerated
Particle size range	5-25 μm	20-116 μm
Nominal compositions	13wt.% Y_2O_3-ZrO_2	8mol% Y_2O_3-ZrO_2

with F4VB Plasma Torch, Sulzer Metco AG, Switzerland) and APS system (PT-2000 with F4MB Plasma Torch, Sulzer Metco AG, Switzerland). Powders were fed into plasma stream by 10-Twin-systems (Plasma-Technik AG, Switzerland) during spraying.

Low pressure plasma spraying was carried out in an argon gas atmosphere under a low-pressure condition. Spray conditions are shown in Table 2. The coating was deposited on a copper plate of dimensions 5 × 7 × 0.3 cm. Prior to spraying, the substrate was grit-blasted with alumina at the pressure of about 0.2 MPa. Preheating of the substrate was also performed using plasma transferred arc just before deposition. A robot (ABB, Sweden) was used to move spray torch for a uniform and reproducible deposition of YSZ layer.

Atmospheric pressure spraying was carried out in an ambient atmosphere and YSZ coating was deposited on an aluminum plate of dimensions 5 × 7 × 0.3 cm as a substrate without preheating. The substrate was also grit-blasted prior to plasma spraying in the same way as in LPPS. APS conditions are also shown in Table 2. After deposition, the substrates were dissolved by nitric acid and sodium hydroxide solutions, respectively, to obtain the freestanding specimens.

2.2 Measurement of the Gas Permeability

The gas permeability was measured using equipment schematically shown in Fig. 2. The pressure in the tube was reduced by a rotary vacuum pump, which produced a pressure difference between ambient atmosphere and the inside of the tube. Once the maximum vacuum state was achieved, the pump was switched off and air leakage through the YSZ layer led to the reduction of the pressure difference. According to the changes of the pressure difference with leakage time, the gas permeability can be estimated. YSZ samples with the thickness of 600~800 μm and the area of about 1.5 cm^2 were used in this experiment. The detail of calculation was shown elsewhere (Ref 6).

2.3 Measurement of the Electrical Conductivity

The electrical conductivity of YSZ coating was measured using potentiostat/galvanostat based on a 3-electrode assembly approach (Fig. 3) (Ref 10). To ensure the measuring area of the circular planar sample, platinum glue was pasted on both sides of the sample with a specific effective area of 1 cm^2 and a thickness of 600~800μm. The pasted sample was dried at 100 °C for 30 minutes and then heated to 850 °C with a heating rate of 5 °C/min and kept at 850 °C for 30 minutes. The reference electrode (RE in Fig. 3) and counter electrode (CE in Fig. 3) were connected to one side of the sample, while working electrode (WE in Fig. 3) was connected to the other side of the sample. In this study, the measurement was conducted in an isothermal condition. The data was collected after 20 min when the furnace temperature reached the prescribed point. According to the linear relationship between current and potential difference, the resistivity and subsequently conductivity was determined (Ref 10).

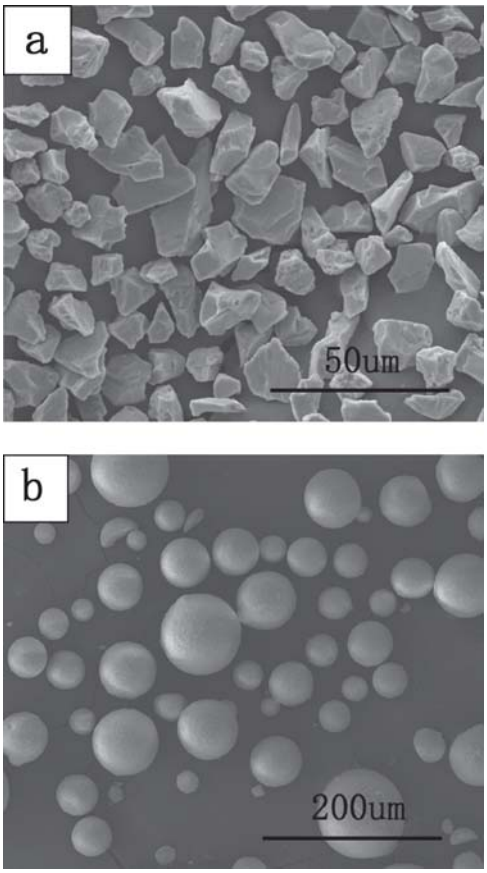

Fig. 1 Feedstock powder morphology: (a) YSZ1 fused-crushed powder, (b) YSZ2 agglomerated powder

Table 2 LPPS and APS spraying parameters used for deposition of YSZ coating

Specimen code	LPPS1	LPPS2	APS1	APS2
Powder	YSZ1	YSZ2	YSZ1	YSZ2
Arc current, A	720	720	600	600
Plasma power, kW	45	45	40	40
Chamber pressure, M/Pa	0.07	0.07	0.1	0.1
Standoff distance, mm	160	160	100	100
Plasma gas flow rate				
Argon, 1/min	40	40	32	35
Hydrogen, 1/min	11	13	11	12
Powder feed rate				
Powder feed rate, g/min	38	15	39	15
Argon powder carrier gas, l/min	3.7	3.7	3.5	3.5
Gun traverse speed, mm/s	200	200	500	500

LPPS, low pressure plasma spraying; APS, atmospheric pressure spraying

2.4 Microstructure Characterization

The phase constitutions of both powder and deposited coating were characterized by x-ray diffraction analysis (XRD-6000, Shimadzu, Japan) using a CuKα radiation. A 2θ scanning rate of 10° min^{-1} was used during test. The microstructure of plasma-sprayed coatings was examined by scanning electron microscopy (Quanta 200, Philips-FEI, Eindhoven, The Netherlands).

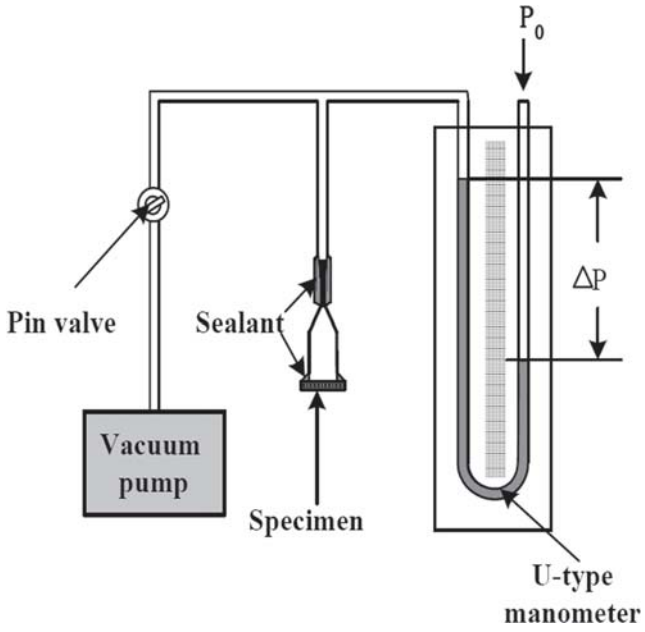

Fig. 2 Schematic of the experimental setup for gas permeability measurement

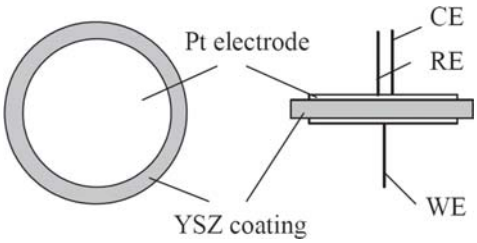

Fig. 3 Schematic of the arrangement of three-electrode assembly for measurement of electrical conductivity of plasma sprayed YSZ electrolyte

3. Results and Discussion

3.1 Microstructure of Plasma-Sprayed YSZ Coatings

Figure 4 shows the XRD patterns of plasma-sprayed YSZ coatings at different conditions in comparison with the starting powders. XRD pattern indicated that the powders consisted of a well-crystallized single cubic zirconia phase. Moreover, all YSZ coatings presented the same cubic phase as that of the powders.

Figure 5 shows typical surface morphologies of YSZ coatings deposited at different conditions obtained by scanning electron microscopy (SEM). The surface morphology suggests that the coatings were composed of well-flattened particles. The microcracks were clearly present in all samples that are inherent in a plasma-sprayed ceramic coating.

Figure 6 shows cross-sectional microstructure of four YSZ coatings. It can be clearly observed that the YSZ coatings deposited with smaller fused and crushed powder presented a dense microstructure, while the coating deposited by YSZ2 powder presented a more porous microstructure than YSZ1 powder. During plasma spraying, sufficient melting and high velocity of spray particle is necessary to deposit a dense coating.

Comparing the two powders, it was clear that particle size of

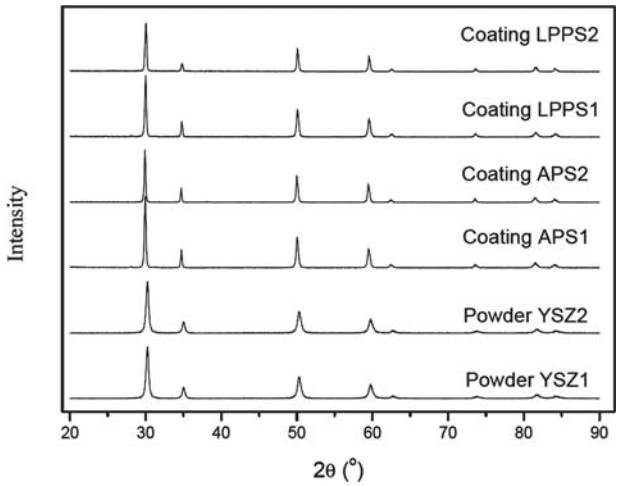

Fig. 4 XRD patterns of the plasma sprayed YSZ coatings in comparison with those of the starting powders

YSZ1 powder is much smaller than that of YSZ2 powder in the current study. Under the same plasma conditions, a smaller particle is more easily heated to melting state compared with a larger particle. Therefore, it is reasonable to achieve a denser coating with YSZ1 powder.

Comparing LPPS1 coating to APS1 coating, it shows that there are less microcracks in the surface of LPPS1 (Fig. 5c) deposit than that in APS1 (Fig. 5a) although it is difficult to indicate which coating has more porosity (Fig. 6a and c). There may be two reasons for this phenomenon. On one hand, the LPPS deposit is maintained at a much higher temperature than in the APS deposit due to the increased interaction between the plasma jet and the substrate (caused by the longer plasma jet), coupled with the absence of convective cooling of the substrate. On the other hand, LPPS can produce higher particle velocity than APS and increased particle velocity causes enhanced flattening and spreading of the droplet.

3.2 Gas Permeability

Figure 7 shows typical change of the pressure difference across the specimen with time. It is obvious that four YSZ coatings presented different performance of gas leakage. With the coatings deposited with smaller YSZ1 powder, the pressure dropped more slowly compared with the YSZ coatings deposited with larger YSZ2 powder.

According to those results, the mean gas permeability was calculated for different coatings. The results are shown in Table 3. It can be recognized that the specific gas permeability of YSZ coatings ranged from $1.32 \times 10^{-17} m^2$ to $2.63 \times 10^{-16} m^2$. Fox et al. (Ref 11) reported a specific gas permeability of 0.6×10^{-16} to 1.8×10^{-16} m^2 for APS 4.9 mol% Y_2O_3-stabilized YSZ coating.

It seems that the present results are reasonable compared with those reported by Fox et al. Moreover, it can be found from present results that powder type has a significant influence on gas permeability of plasma-sprayed YSZ coatings. The gas permeability of YSZ coatings deposited by YSZ1 powder is almost one order lower than the YSZ coatings deposited by YSZ2 powder. Moreover, with YSZ1 powder of small particle size, LPPS coating is more gas tight than APS coating. The specific gas permeability of LPPS1 specimen reached a value of 1.3×10^{-17}

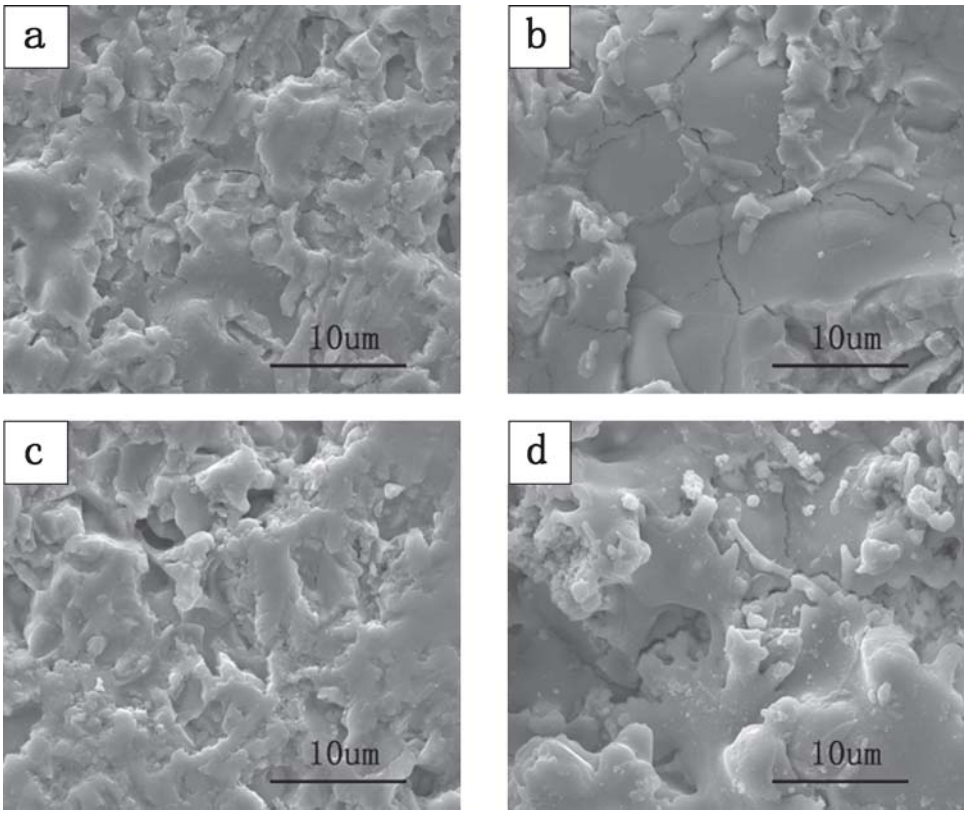

Fig. 5 SEM surface morphologies of the YSZ coatings: (a) APS1, (b) APS2, (c) LPPS1, (d) LPPS2

m^2, which is only about one third of that of APS sample with the same powder. Therefore, deposition of YSZ coating by LPPS with small powders can easily achieve high gas tightness necessary for operation of SOFC. The microstructure examination of plasma-sprayed YSZ coatings mentioned previously clearly showed that a denser microstructure was achieved using small powder. Therefore, the lower gas permeability is attributed to dense microstructure of the coating.

3.3 Electrical Conductivity of Plasma-Sprayed YSZ Coatings

Figure 8 shows the electrical conductivity of YSZ coatings measured at different temperatures. The electrical conductivity of all sprayed specimens increased with the increase of measurement temperatures. The electrical conductivity of the LPPS YSZ coatings is a little higher than that of APS coatings at high temperature and a little lower at lower temperature. The electrical conductivity of APS sample increased from 0.00068 S/cm to 0.038 S/cm when the test temperature increased from 600 to 1000 °C. Meanwhile, the electrical conductivity of LPPS sample deposited with YSZ1 powder increased from 0.00063 S/cm to 0.043 S/cm with the corresponding temperature increment. This fact indicates that the electrical conductivity of LPPS YSZ coating deposited by YSZ1 powder was improved by 20% at 1000 °C compared with APS YSZ coatings. From the results reported by Yamamoto (Ref 12) and Ivers-Tiffee et al. (Ref 13), 8 mol% Y_2O_3-stabilized YSZ bulk shows an electrical conductivity from 0.14 S/cm to 0.18 S/cm at 1000 °C. Previous investigations showed that the electrical conductivity of LSM (Ref 14) and YSZ (Ref 6) coatings deposited by APS was one-fifth to one=third of the corresponding bulk materials. The result obtained in this study is consistent with those previous findings. Therefore, the electrical conductivity of plasma-sprayed coating will be dominated by lamellar structure and bonding condition between lamellae in the coating. Moreover, it can be found that the electrical conductivity of LPPS YSZ coating deposited with YSZ2 powder is lower than that with YSZ1 powder. The previous study has revealed that powder structure presents a significant influence on coating microstructure and electrical conductivity (Ref 15).

With an agglomerated powder, although the powder flowability is significantly improved, incomplete melting will result in the formation of additional nonbonded interfaces that act as the barrier for ion transportation. As a result, it is more difficult to deposit a coating of a high electrical conductivity with agglomerated powder.

The temperature dependence of the ionic conductivity of zirconia-based electrolytes has been investigated extensively. Generally, the measured conductivity data is analyzed according to the traditional Arrhenius equation (Ref 16):

$$\sigma = \sigma_0 \exp\left(-\frac{E}{kT}\right) \quad \text{(Eq 1)}$$

where E is the activation energy for ion conduction, and σ_0 is a material constant and k is Boltzmann constant. Arrhenius plot for different YSZ coatings is shown in Fig. 9. From those results, the plot can be fitted by two straight lines rather than one single line. Non-Arrhenius behavior has been reported for Zirconia-

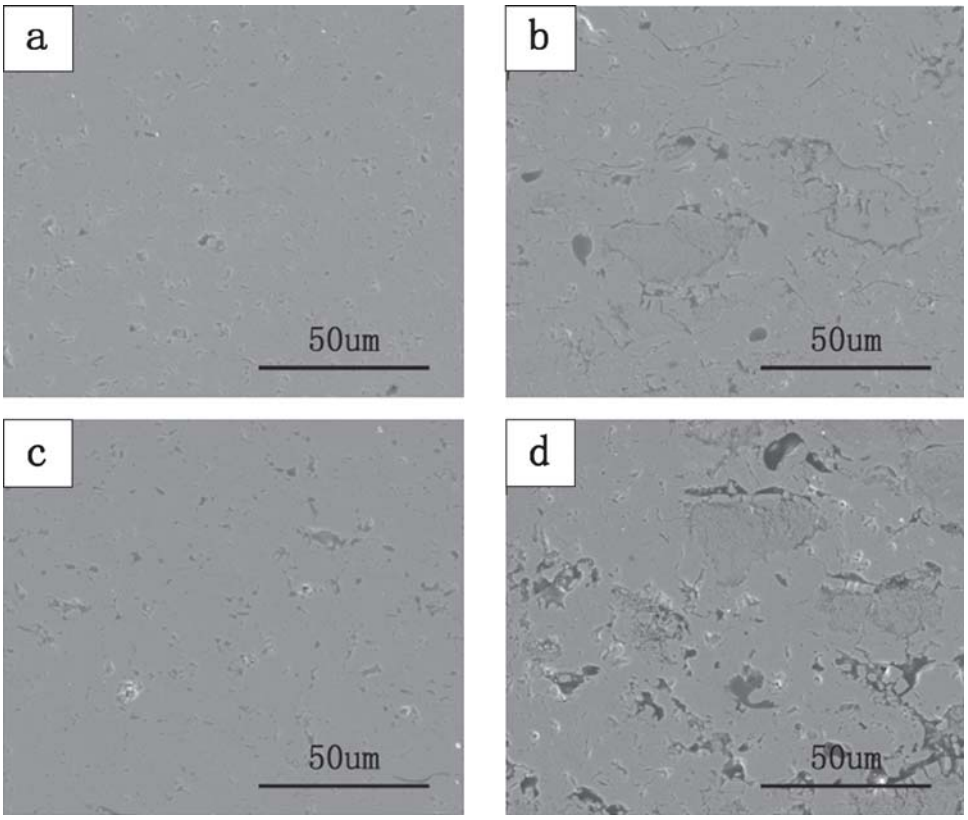

Fig. 6 SEM microstructure of YSZ coatings (a) APS1, (b) APS2, (c) LPPS1, (d) LPPS2

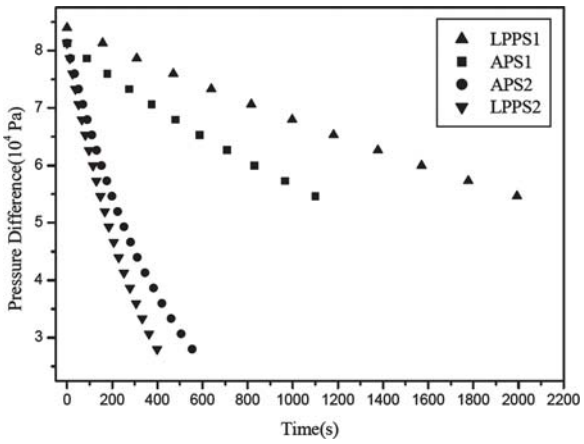

Fig. 7 Change of the pressure difference against leakage time for YSZ specimens plasma deposited with different conditions

based coatings (Ref 17-19). A commonly accepted method to study the nonlinear Arrhenius behavior is to fit the experimental data by two respective straight lines in both the lower and the higher temperature ranges. There are two explanations for this phenomenon. According to Ref. 17, there are two kinds of oxygen vacancies in the materials: one being free and the other forming clusters. It was suggested that at the lower temperature range, all the oxygen vacancies are associated with the doping cations to form clusters, and the activation energy for conduction, E, in this temperature range can be described as the sum of the disassociation energy, E_a, and the migration energy, E_m, for oxygen vacancies. At the higher temperature range, it was usually assumed that all the oxygen vacancies are free and the activation energy reflects only the migration energy for the oxygen vacancies. According to our previous study (Ref 19), this is due to the change in dominance of electrical conductivity from grain boundary impedance at low temperature to intragrain impedance at higher temperatures.

Table 3 Specific gas permeability of different plasma-sprayed coating

APS1	APS2	LPPS1	LPPS2
3.09×10^{-17} m^2	1.16×10^{-16} m^2	1.32×10^{-17} m^2	2.63×10^{-16} m^2

The detailed examination revealed that the activation energy of both LPPS and APS deposited YSZ samples at high temperatures was lower than that at low temperature range. As shown in Fig. 9, the activation energy of the LPPS1 coating and APS1 coating specimen were about 1.01 eV and 1.14 eV, respectively, the temperatures lower than 700 °C, while they decreased to 0.88 eV and 0.85 eV at temperatures above 700 °C.

The activation energy of APS deposited YSZ sample was higher than that of LPPS specimen at low temperatures and very similar at higher temperatures. This difference may be resulted from the intragranular features of the APS and LPPS deposited YSZ coating. Further study is necessary to clarify the reasons behind this difference.

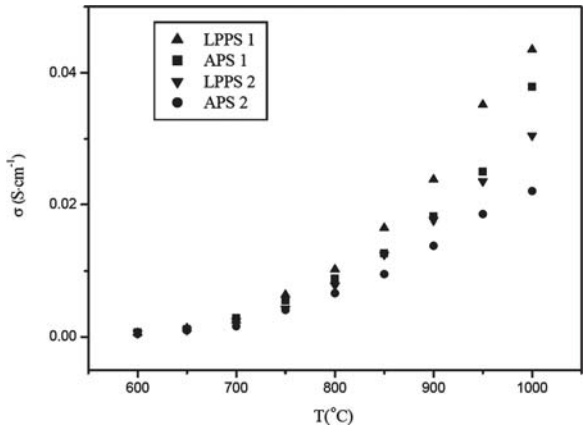

Fig. 8 Effect of temperature on the electrical conductivity of the plasma sprayed YSZ coating by dc approach

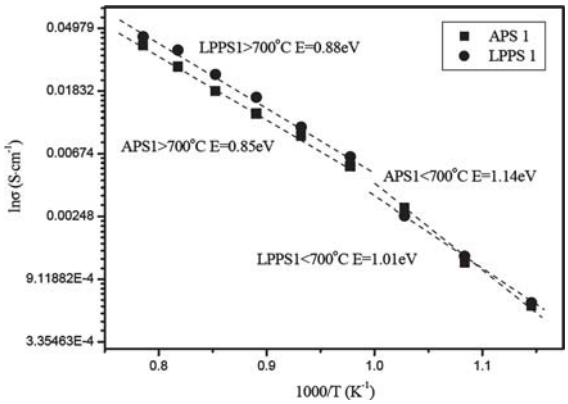

Fig. 9 σ versus 1/T plots for the electrical conductivity for the test specimens

4. Conclusions

Powder structure and plasma spraying atmosphere have significant influence on YSZ coating density. The present results showed that a dense YSZ coating was deposited using a fused-crushed powder by both LPPS and APS compared with YSZ coatings deposited using agglomerated powder. The gas permeability of plasma-sprayed YSZ coating using small fused-crushed powder is one order lower in magnitude than that using larger agglomerated powder. Furthermore, the specific gas permeability of the LPPS YSZ coating was lower than that of APS YSZ coating.

The electrical conductivity of YSZ coating deposited by LPPS with fused-crushed powder of small particle size was 0.043 S/cm at 1000 °C, which is 20% higher than that of APS YSZ coating. It was also found that the activation energy for ion conduction of both APS and LPPS deposits changed when temperature was increased from lower temperature to about 800 °C. The activation energy of the APS coating was 1.14 eV at temperature range less than 700 °C and 0.85 eV at temperature above 700 °C while that of LPPS were 1.01 eV and 0.88 eV, respectively. The change of activation energy suggests that the ion transportation dominants change with change of temperature.

Acknowledgments

One of the authors (C. Zhang) thanks the co-tutors scholarship (Bourse doctorales en cotutelle franco-chinoise) of French Ministry of Education. The authors are grateful to Dr. Shengqiang Fan of Xi'an Jiaotong University for his assistance of XRD and Dr. Yazhe Xing of Xi'an Jiaotong University for his assistance of electrical conductivity measurement. The authors also thank Miss Lydie Lahoupe of Université de Technologie de Belfort-Montbéliard for her help in the preparation of the metallographic samples.

References

1. F.M.B. Marques and L.M. Navarro, Performance of Double Layer Electrolyte Cells Part I: Model Behavior, *Solid State Ionics,* 1996, **90,** p 183-192
2. K.R. Sridhar and B.T. Vaniman, Oxygen Production on Mars Using Solid Oxide Electrolysis, *Solid State Ionics,* 1997, **93,** p 321-328
3. J. Will, A. Mitterdorfer, C. Kleinlogel, D. Perednis, and L.J. Gauckler, Fabrication of Thin Electrolytes for Second-Generation Solid Oxide Fuel Cells, *Solid State Ionics,* 2000, **131,** p 79-96
4. M. Lang, R. Henne, S. Schaper, and G. Schiller, Development and Characterization of Vacuum Plasma Sprayed Thin Film Solid Oxide Fuel Cells, *J. Therm. Spray Technol,* 2001, **10,** p 618-624
5. S. Rambert, A.J. McEvoy, and K. Barthel, Composite Ceramic Fuel Cell Fabricated by Vacuum Plasma Spraying, *J. Eur. Ceram. Soc,* 1999, **19,** p 921-923
6. C.-J. Li, X.-J. Ning, and C.-X. Li, Effect of Densification Processes on the Properties of Plasma-Sprayed YSZ Electrolyte Coatings for Solid Oxide Fuel Cells, *Surf. Coat. Technol,* 2005, **190,** p 60-64
7. A. Notomi and N. Histome, Application of Plasma Spraying to Solid Oxide Fuel Cell Production, *Pure Appl. Chem.,* 1996, **68,** p 1101-1106
8. G. Schiller, R.H. Henne, M. Lang, R. Ruckdaschel, and S. Schaper, Development of Vacuum Plasma Sprayed Thin-Film SOFC for Reduced Operating Temperature, *Fuel Cells Bull.,* 2000, **3,** p 7-12
9. C.-J. Li, C.-X. Li, and Y.-Z. Xing, M. G, G.-J. Y, Effect of YSZ Electrolyte Thickness on the Characteristics of Plasma-Sprayed Cermet Supported Tubular SOFC, *Solid State Ionics,* 2006, **177,** p 2065-2069
10. X.-J. Ning, "Study on the Fabrication of Zirconia Based Electrolyte for SOFC by Atmospheric Plasma Spraying," Ph.D. Thesis, Xi'an Jiaotong University, 2005, p 38-41, in Chinese
11. A.C. Fox and T.W. Clyne, Oxygen Transport by Gas Permeation through the Zirconia Layer in Plasma Sprayed Thermal Barrier Coatings, *Surf. Coat. Technol,* 2004, **184,** p 311-321
12. O. Yamamoto, Solid Oxide Fuel Cells: Fundamental Aspects and Prospects, *Electrochim. Acta,* 2000, **45,** p 2423-2435
13. E. Ivers-Tiffee, A. Weber, and D. Herbstritt, Materials and Technologies for SOFC-Components, *J. Eur. Ceram. Soc.,* 2001, **21,** p 1805-1811
14. C.-J. Li, C.-X. Li, and M. Wang, Effect of Spray Parameters on the Electrical Conductivity of Plasma-Sprayed $La_{1-x}Sr_xMnO_3$ Coating for the Cathode of SOFCs, *Surf. Coat. Technol.,* 2005, **198**(1-3), p 278-282
15. X.-J. Ning, C.-X. Li, C.-J. Li, G.-J. Yang, Effect of Powder Structure on Microstructure and Electrical Properties of Plasma-Sprayed 4.5mol% YSZ Coating, *Vacuum*, in proof
16. Z.-X. Lin, Z.-K. Guo, and C.-W. Sun, *Rapid Ion Conductor-Foundation, Materials, Application*, Shanghai Science Technology Press, Shanghai, 1983, p 46-87, in Chinese
17. J.-H. Gong, Y. Li, Z.-L. Tang, Y.-S. Xie, and Z.-T. Zhang, Temperature-Dependence of the Lattice Conductivity of Mixed Calcia/yttria-Stabilized Zirconia, *Mater. Chem. Phys.,* 2002, **76,** p 212-216
18. I. Kosacki, H.U. Anderson, Y. Mizutani, and K. Ukai, Nonstoichiometry and Electrical Transport in Sc-Doped Zirconia, *Solid State Ionics,* 2002, **152-153,** p 431-438
19. C.-X. Li, C.-J. Li, H.-G. Long, C. Zhang, Y.-Z. Xing, and H.-L. Liao, Characterization of Atmospheric Plasma-Sprayed Sc_2O_3-ZrO_2 Electrolyte, *Solid State Ionics,* 2006, **177,** p 2149-2153